Analyst

Accepted Manuscript

ROYAL SOCIETY OF CHEMISTRY

www.rsc.org/analyst

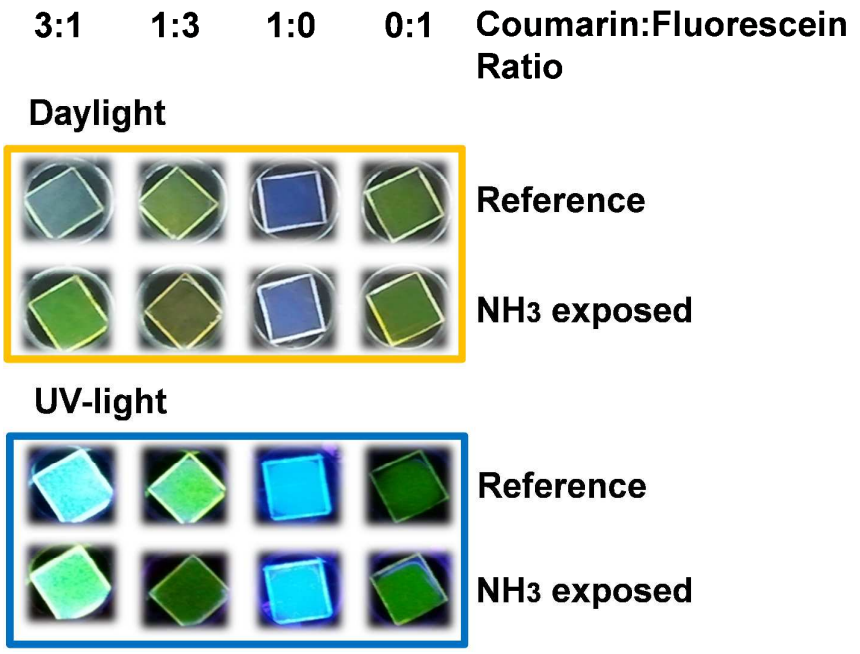

The incorporation of a FRET-based sensing system into an organic modified silica matrix resulted in a quantitative and reversible optical ammonia gas sensor with a linear response.

Analyst

RSCPublishing

ARTICLE

Coumarin meets Fluorescein: A Förster Resonance Energy Transfer enhanced optical Ammonia Gas Sensor

Cite this: DOI: 10.1039/xoxxoooooox

Received ooth January 2012,
Accepted ooth January 2012

DOI: 10.1039/xoxxoooooox

www.rsc.org/

Susanne Widmer[a,b], Marko Dorrestijn[a], Agathe Camerlo[a], Špela Korent Urek[c], Aleksandra Lobnik[c], Catherine E. Housecroft[b], Edwin C. Constable[b] and Lukas J. Scherer*[a]

This study focuses on the development of an optical ammonia gas sensor, the sensing mechanism of which is based on Förster resonance energy transfer (FRET) between coumarin and fluorescein. The dyes were immobilized into an organically modified silicate matrix during polymerizing methyltriethoxysilane with trifluoropropyltrimethoxysilane on a poly(methyl methacrylate) substrate. The resulting dye-doped xerogel films were exposed to different gaseous ammonia concentrations. A logarithmic decrease of the coumarin fluorescence emission band at 442 nm was observed with increasing gaseous ammonia concentrations, which was due to enhanced FRET between coumarin and fluorescein. The coumarin/fluorescein composition was optimized in order to obtain the best ammonia sensitivity. First experiments in a flow cell gas sensor setup demonstrated a sensitive and reversible response to gaseous ammonia.

1 Introduction

A large number of ammonia gas sensors have been reported, demonstrating the continuing demand for efficient detection systems. A range of methods is available for monitoring gaseous ammonia, including electrochemical devices, solid-state sensors, spectroscopic techniques and conducting polymers.[1,2-4] Several optical ammonia gas sensors have been reported, based on spectrophotometric ammonia detection by monitoring a change in absorption or fluorescence.[5-12] Optical sensors based on analyte sensing fluorescent dyes show better sensitivity and selectivity compared to those based on absorbing spectroscopy because fluorescent measurements have a larger number of experimental parameters (λ_{ex}, λ_{em}, $\tau_{lifetime}$ etc.) available for manipulation compared to absorption measurements.[10] The choice of fluorescein derivatives as the analyte sensing molecule is reasonable since the dye has high quantum yields, good photostability, a large Stokes shift and possible reactive sites in the skeleton for covalent modification.[9,10,13-15]

We now report a sol based optical gas sensor, which quantitatively detects ammonia. The sensing mechanism is based on Förster resonance energy transfer (FRET) between coumarin and fluorescein, a phenomenon that describes the nonradiative transfer of energy between two chromophores.[16] Few FRET-based optical chemosensors for the detection of ammonia have been reported[17-20] and the advantages have been highlighted as they can generate dual or multiple emissions under a single wavelength excitation, resulting in more effective ratiometric detection in comparison to those that need two separate excitation wavelengths.[21] Furthermore, their design can easily be modified by varying the FRET components. For this preliminary study, fluorescein has been chosen as the analyte sensitive acceptor dye to relate to established benchmarks.[9,10] We demonstrate that by implementing a FRET system, the sensitivity becomes linear over a wide ppm range.

2 Experimental details

2.1 Chemical reagents and materials

Fluorescein, 7-diethylamino-4-methylcoumarin, 3,3,3-trifluoro-propyltrimethoxysilane, methyltriethoxysilane and hydrochloric acid (37%) were purchased from Sigma Aldrich. Ethanol in HPLC grade was obtained from Fluka. All chemicals were used without further purification. Custom mixed gases 96.2 ppm ± 2% rel. NH_3 in N_2 (≥ 99.8%), 0.101 ± 1% rel. NH_3 in N_2 and pure N_2 gas were acquired from Carbogas. Poly(methyl methacrylate) (PMMA) microscope slides (25 mm x 75 mm x 1 mm) and a 0.5 mm thick PMMA foil were purchased from microfluidic ChipShop.

2.2 Sol preparation

Coumarin/fluorescein sols were prepared by dissolving the desired amount (6.25, 12.5, 25, 37.5, 50, 62.5 and 75 µmol) of the dyes in 5 ml of ethanol. After sonication (UltrasonicCleaner from VWR, 45 kHz, 80 W) of the solution for 10 min at room temperature, methyltriethoxysilane (1.793 ml, 9 mmol) and 3,3,3-trifluoropropyltrimethoxysilane (0.576 ml, 3 mmol) were added. After a further 10 min of sonication, 0.1 M HCl (0.08

ml) and water (0.64 ml) were added to the solution. The sol was sonicated for another 20 min and then aged for 24 h at room temperature ("aged sol"). Figure 1a illustrates the sol preparation pathway.

2.3 Xerogel preparation

For fluorescence and UV-visible spectroscopy measurements Five µl of aged sols were solvent cast on PMMA films (4.5 mm x 4.5 mm x 0.5 mm) with a micropipette. The sol-coated PMMA substrates were dried in an oven at 70 °C for 12 days to ensure stable gel composition. The scheme in Figure 1b depicts the xerogel film preparation pathway.

For gas sensor measurements Different amounts (20, 40 and 60 µl) of aged sols were solvent cast onto PMMA films (15 mm x 15 mm x 1 mm) with a micropipette. The sol was homogenously distributed over the substrate with the micropipette tip. After 10 min drying in air, the sol-coated PMMA substrates were dried in an oven at 70 °C for 12 days.

2.4 Characterization methods

ATR-IR, UV-visible and fluorescence spectroscopy ATR-IR spectra were obtained from a FT-IR Biorad spectrophotometer equipped with a Specac Golden Gate bridge. Spectra of the sol solution and pestled xerogel were recorded.

Fluorescence spectra were recorded in the range of 385 – 650 nm on a Biorad Fluorescence spectrophotometer. Both the excitation and emission slit were set to 10 nm and the detector voltage was set to low. The small xerogel-coated PMMA plates were horizontally pinched into the wells of a microtitre wellplate at the same height. The plates were exposed to ammonia gas by adding 20 µl of the desired aqueous ammonia solutions to the well bottom by a micro syringe. The well plate was then covered by the corresponding lid and enwrapped with parafilm. Before each fluorescence measurement, the loaded wellplate was stored in a conditioned room (21 °C, 50% rel. air humidity) for 30 min to ensure same measurement conditions. The ammonia vapour concentrations within the wells were calculated based on the reported partial pressure of ammonia.[22,23]

UV-visible absorption spectra were measured between 300 and 800 nm on a Biorad spectrophotometer with a slit width of 1.0 nm. The experimental procedure was similar to the fluorescence experiments described in the previous paragraph.

Refractive index measurement Refractive index measurements on the sols were performed on a device from Atago equipped with an illuminator. The refractive index of undoped solid xerogel was determined using certified refractive index liquids made by Cargille labs.

Contact angle measurement Water contact angle measurements were performed with a contact angle measuring system from Krüss (G10). The value was calculated from the average of five measurements. The droplet size was 5 µl.

Rheometry measurement Viscosity measurements were performed on a plate rheometer from Anton Paar (Physica MCR 301). The change in viscosity of the sol upon heating was measured by placing a vial containing a 24 h aged sol in a preheated oven at 70 °C. The shrinking and gelling sol, due to solvent evaporation and heat, was measured every 30 min.

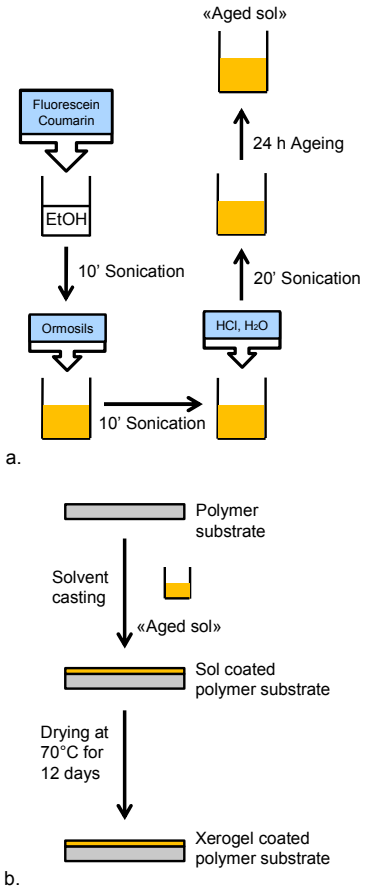

Fig. 1 a.: Sol preparation pathway; b.: Xerogel film preparation pathway.

Profilometry measurements Profilometry experiments were performed with a Vecco Dektak 150 device to determine the xerogel film thickness. Before solvent-casting, two opposite corners of the 15 mm x 15 mm x 1 mm PMMA substrate were covered with tape. The sol was then solvent cast and homogenously distributed over the whole substrate with the micropipette tip. After drying for 12 days, the tapes were carefully removed to obtain a smooth xerogel borderline. The stylus was placed on one xerogel corner and moved over the coated area towards the uncoated opposite corner. For evaluation of the thickness, the profile average with standard deviation was calculated. The given xerogel thicknesses were calculated from the average of 5 measured plates.

Porosity measurements Nitrogen adsorption isotherms were measured at 77 K using a NOVA 3000e Surface Area and Pore Size Analyzer from Quantachrome instruments. Before analysis, the sample was degassed at room temperature for 16 h.

2.5 Gas sensor

Laboratory set-up for testing the ammonia sensing probes Xerogel-coated plates were placed in a flow cell as shown in Figure 2. The plates were illuminated from the top by a 0.4 W UV-LED of peak wavelength 385 nm (FWHM bandwidth 10 nm) purchased from Thorlabs. To measure fluorescence emission, the photodetector was placed orthogonal to the incoming radiation, the PMMA sample plate acting as a

waveguide. Additionally, an optical band-pass filter was placed in front of the detector, which had a 90% transmission band of 415 – 455 nm provided by Semrock (FF02-435/40-25). The inside of the flow cell was painted black to reduce reflections of the direct light. Electronic readout was based on a phototransistor circuit and a LabView-controlled digital multimeter. The time-dependent voltage signal, which was proportional to the emitted light intensity, was post-processed in LabView using a low-pass filter and baseline correction. The flow cell was connected to gas supplies as depicted in Figure 3. The gas flow could be switched between ammonia/nitrogen mixture and nitrogen using manual valves (3). During the experiments, the flow rate (800 ml ± 50 mL/min), the temperature (20 ± 2 °C), and the humidity (< 2%) were monitored in the line using a CMOSens EM1 (Sensirion) and an MSR 145 (Sensirion) respectively.

Measurement and measurement evaluation Before each measurement, the system was flushed with N_2 gas for 5 min. An experiment always started with a 600 – 900 s N_2 gas flush followed by flush of a NH_3 gas mixture. Normally, at least five cycles with NH_3 response and N_2 recovery were measured to ensure system stabilisation and repeatability of the experiments. Response as well as recovery time were kept constant at 35 min. The amplification of the electronic was constant for each measurement. The drift was corrected by fitting a double exponential equation to the turning point of each cycle (highest point of the signal recovery with N_2 gas). The signal noise was reduced by using a fifth order Butterworth low-pass filter with 3 mHz cut-off frequency.

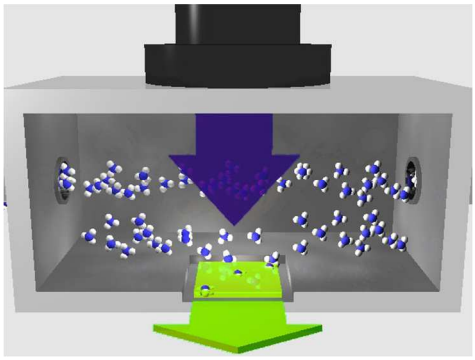

Fig. 2 Rendered impression of the flow cell showing a xerogel coated plate (shown in green) in a recessed area in the floor. The plate is illuminated from the top by a UV-LED (violet arrow) through a UV-transparent window. Fluorescence emission (green arrow) is measured through an opening in the front of the cell.

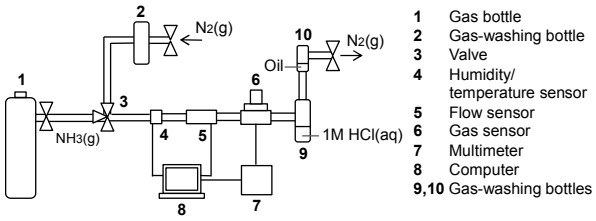

Fig. 3 Schematic of the experimental setup.

3 Results and Discussion

3.1 Sensing film preparation

Sol-gel materials offer several advantages including optical transparency from the ultraviolet to infrared wavelengths as well as chemical and thermal stability.[24] Another benefit of the sol-gel process is the possibility of simple chemical doping of the material by adding the desired dye molecules to the precursor sol solution. Upon polymerization of the precursors, the dyes are immobilized into the silica matrix.[25] Ormosil sol-gels were chosen as matrix materials since they are more hydrophobic compared to inorganic sol-gels[26-28] which improves the cross-sensitivity of the gas sensor towards water. The fluorinated xerogels described here have a water contact angle of 90 ± 1° indicating the increased hydrophobicity. Other reported xerogel-based sensors showed a significant improvement of their sensitivity towards gaseous CO_2 and O_2 upon the integration of trifluoropropyltrimethoxysilanes.[29-31] Furthermore, the more rigid networks of ormosil xerogels can result in less photodegradation of the dyes.[32,33] The kind of ormosil precursors can significantly affect the response to ammonia because of varying ammonia permeability and xerogel polarity.[18,26,34,35] In this study, the focus lies on the optimization of the FRET sensing mechanism occurring within the reported xerogels followed by fluorescence spectroscopy.

Sol-gels and xerogels were prepared using standard hydrolytic methods. The formation of the sol-gel as a result of hydrolysis and condensation results in an increase in viscosity. Rheometry measurements showed that the viscosity of the prepared sols remained constant at room temperature even at longer ageing times, indicating that the condensation reaction proceeds slowly. In general, at pH < 7 the rate of the condensation reaction is limited by the lack of available hydroxide anions.[36] The polymerization was finally induced by heating the sol to 70 °C. The condensation degree during curing at 70 °C was followed by rheometry measurements. The thermal polymerization resulted in an increase in viscosity as illustrated in Figure 4. The increase in viscosity is small for the first 100 min but significant between 120 and 170 min indicating that the main polymerization starts during this time range. After 170 min, the sol-gel was too rubbery to be accurately measured by a plate rheometer.

Organofunctional alkoxysilanes are often used to reduce the degree of cross-linking of the material which often leads to less capillary stress during solvent evaporation and results in crack-free and more flexible sol-gel films.[25,27-40]

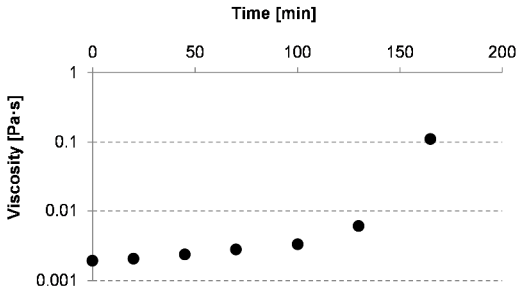

Fig. 4 Plot showing the increase in viscosity due to condensation at 70 °C.

Twelve days drying at 70 °C of solvent cast acid catalysed sol on the PMMA substrate resulted in fracture free (Wallner lines) homogenous xerogel films. Coumarin/fluorescein-doped xerogels showed an increase in fluorescence emission at 442 nm and a decrease in fluorescence emission at 500 – 540 nm during the first 8 to 10 days of drying when excited at 375 nm. In order to achieve constant fluorescence emission, a curing time of 12 days was necessary.

ATR-infrared spectroscopy is frequently used to monitor different stages of sol-gel processing of silica gels and is an elegant method to verify the formation of siloxane bridges upon polymerization.[41] The main change in ATR-IR spectra upon thermal sol to xerogel evolution is based on the ethanol and ormosil consumption and the formation of Si–O–Si bonds.[41] This was detected by the disappearance of the ethanol and ormosil related bands at 3330, 2970, and 1380 cm^{-1} and by the simultaneous formation and intensification of the siloxane (Si–O–Si, Si–O) related bands at 1000, 900 and 770 cm^{-1} after 12 days curing time.

3.2 Choice of the dyes and sensing mechanism

Fluorescein derivatives have been used as sensing species displaying linear dependency over wide ranges of ammonia concentrations.[6,9,10] Depending on the ambient pH value, fluorescein exists in cationic, neutral, mono-ionic or dianionic forms or as a mixture of them.[14] The acidity constants in solution reported for fluorescein are in the range of $pK_{cationic}$ = 2.00 – 2.25, $pK_{neutral}$ = 4.23 – 4.4 and $pK_{mono\text{-}ionic}$ = 6.31 – 6.7,[13,14,42] depending on the specific conditions and measurement techniques. Absorption as well as emission spectra are dependent on the pH of the environment due to the presence of species in different protonation states.[14] Absorption spectra of the fluorescein doped xerogels after production showed that fluorescein existed in a mixture of neutral (absorption shoulder at 435 and side maximum about 483) and mono-anionic forms (absorption peak at 457 and about 483 nm). The fluorescence emission of these claddings occurred between 500 and 600 nm. The two main emission peaks of the xerogel in the absence of ammonia are at 515 and 542 nm (Figure 5). The quantum yields and molar absorptivities of neutral and mono-anionic fluorescein (ΦF = 0.3, ΦF_- = 0.37)[14] are reported to be small resulting in moderate fluorescence emission, which is in accordance to our findings (Figure 5 and 6). Ammonia (pK_b = 9.2) is detected by deprotonation of the fluorescein derivatives resulting in a fluorescence enhancement between 500 – 600 nm when excited at 481 nm (Figure 5), because the resulting deprotonated dianionic molecule is fully conjugated. Ammonia treated xerogels exhibited a much stronger absorption band at 492 nm with a shoulder at 455 nm and an emission band at 542 nm (Figure 5 and 6). The main fluorescein emission band at 515 nm disappeared while the signal at 542 nm became the main emission peak when exposed to ammonia, indicating that the dianionic species became the dominant species. The high intensity of the emission is in correspondence with the high reported quantum yield (ΦF_{2-} = 0.93)[14] and the high molar absorptivity of the dianionic fluorescein form. The overlap of the decreasing signal at 515 nm and the increasing signal at 542 nm when exposed to ammonia made quantitative analysis of the region between 500 – 600 nm difficult (Figure 5). Furthermore, the spectral evaluation revealed that the increase in fluorescein fluorescence intensity was not logarithmic when excited at 481 nm.

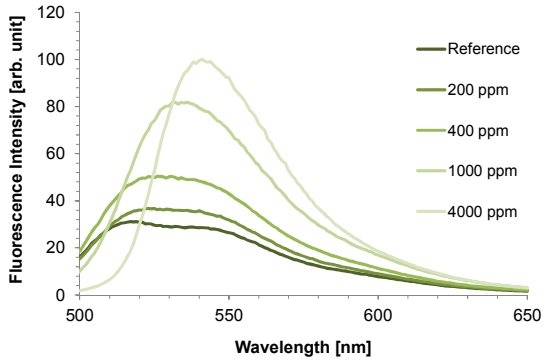

Fig. 5 Change in fluorescence emission spectra for a fluorescein doped xerogel (sol composed of 25 µmol fluorescein) upon ammonia exposure (ex: 481 nm).

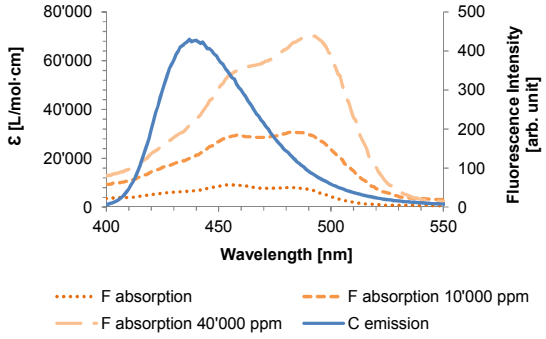

Fig. 6 Increasing spectral overlap of coumarin (C) emission and fluorescein (F) (mono- and dianion) absorption due to exposure to different ammonia gas concentrations given in ppm. The spectra were obtained from xerogels whose sols were doped with 25 µmol coumarin and 12.5 µmol fluorescein.

Due to the unsatisfying sensor characteristics of fluorescein xerogels, we decided to incorporate a FRET sensing mechanism (Figure 7). FRET describes the transfer of the excited state energy from an initially excited donor (D) to an acceptor (A). This process occurs if the emission spectrum of D overlaps with the absorption spectrum of A. The emission wavelength of the newly incorporated second dye, coumarin, overlaps strongly with the absorption wavelength of fluorescein (Figure 6) and FRET between these two dyes is anticipated.[16] The efficiency of the energy transfer in FRET is dependent on the distance between the donor (coumarin) and the acceptor (fluorescein), as well as on the relative orientation of the donor emission dipole moment and the acceptor absorption dipole moment.[16] Furthermore, the Förster distance R_0 depends on the overlap of the donor emission spectrum with the acceptor absorption spectrum and their mutual molecular orientation as expressed by the following equation:[16]

$$R_0^6 = \frac{9Q_0(ln10)\kappa^2 J}{128\pi^5 n^4 N_A}$$

Q_0 describes the fluorescence quantum yield of the donor (coumarin) in absence of the acceptor (fluorescein) which was not quantified. The refractive index n of an undoped xerogel (n = 1.404) and the dipole orientation factor κ are constant. The only variable factor in our system is the spectral overlap J. The spectral overlap of coumarin emission and fluorescein absorption bands varied with the ammonia concentration as a

consequence of deprotonation of the fluorescein. When coumarin/fluorescein xerogels were excited at the coumarin excitation wavelength of 375 nm, the emission of fluorescein between 500 – 600 nm showed also a disappearance of the signal at 515 nm as in pure fluorescein xerogels (Figure 8). An additional emission band at 442 nm was observed which corresponds to the emission of coumarin since not all emission energy is transferred for the excitation of fluorescein. When these xerogels were exposed to ammonia, the intensity of this coumarin emission band decreased. This is a result of a more efficient FRET, since the spectral overlap increased as the fluorescein dianion is formed (Figure 6). The enhanced FRET efficiency resulted in less overall coumarin emission between 400 – 500 nm, as more coumarin emission energy is transferred for fluorescein excitation.

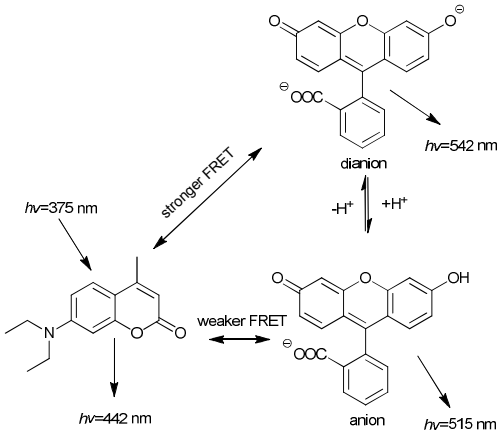

Fig. 7 Schematic of the sensing mechanism.

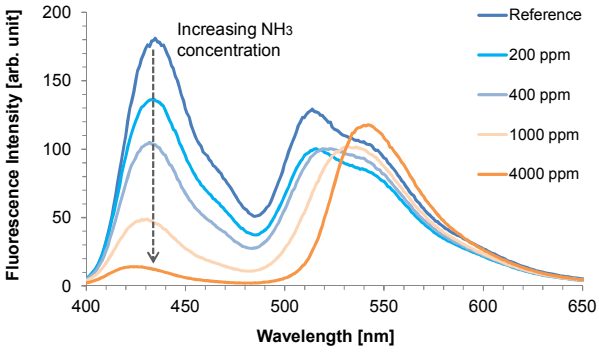

Fig. 8 Fluorescence emission spectra observed of a 1:1 coumarin:fluorescein xerogel (sol composed of 25 µmol coumarin and 25 µmol fluorescein) upon exposure to different amounts of gaseous ammonia (ex. 375 nm).

The signal at 442 nm was much better suited for detection purposes than the fluorescein emission between 500 – 600 nm since it was much more sensitive to changes of the ammonia concentration and a clear decrease in intensity was observed with increasing ammonia concentration (Figure 8). This trend was observed for the entire ammonia concentration studied. Figure 9 shows that the coumarin fluorescence emission decreased logarithmically at 442 nm over the entire region from the lowest ppm concentration (40 ppm) to the highest ammonia concentration measured (40,000 ppm).

In order to optimize the response towards ammonia, different coumarin/fluorescein dye ratios were investigated. The decrease of the emission signal at 442 nm upon exposure to ammonia was followed by fluorescence spectroscopy. Figure 10 shows the decrease of the emission signal of different coumarin/fluorescein ratios at this wavelength when exposed to 10'000 ppm ammonia upon excitation at 375 nm. Since fluorescein is not excited at 375 nm, no change in fluorescein emission from 500 to 600 nm due to ammonia exposure was observed in gels containing only fluorescein. Only coumarin doped xerogels showed an intense emission at 442 nm, but the change in emission intensity due to ammonia was relatively low and not quantitative for different ammonia concentrations, even at higher coumarin concentrations.

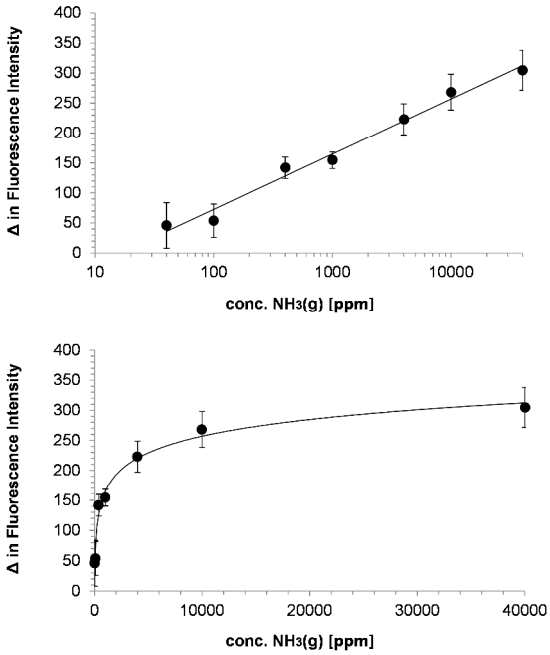

Fig. 9 Top: Plot showing the difference in loss of fluorescence intensity at 442 nm of the most sensitive xerogel (sol composed of 25 µmol coumarin and 6.25 µmol fluorescein) when exposed to different gaseous ammonia concentrations and excited at 375 nm; bottom: Semi-log plot showing the linear trend.

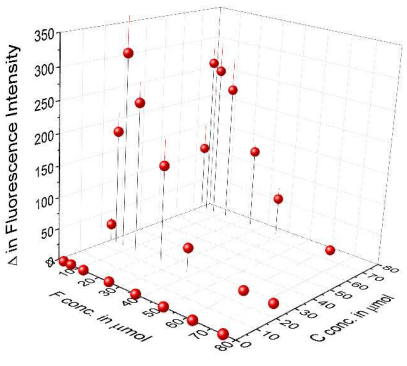

Fig. 10 3D plot illustrating the loss of fluorescence for different coumarin:fluorescein ratios upon ammonia exposure (10'000 ppm). The given concentrations refer to the concentrations in the starting sol solution. The samples were excited at 375 nm, and the emission measured at 442 nm.

The dye mixtures exhibited different responses to ammonia. At constant coumarin concentration, it is observed that at low fluorescein content an increasing fluorescein concentration has a positive influence on the ammonia sensitivity. However, greater amounts of fluorescein (more than 20 µmol in the initial sol solution) lead to an overall reduced FRET as the spectral overlap becomes too dominant. On the other hand, a higher coumarin concentration did not result in a signal benefit due to self-quenching. The most sensitive xerogel resulted from the sol that was composed of 25 µmol coumarin and 6.25 µmol fluorescein. No rational explanation was found for this correlation.

The fluorescence spectra of the dye-doped xerogel films were measured over 6 months during which no significant change in ammonia sensitivity was observed.

3.3 Gas sensor results

In order to investigate the response behaviour, reproducibility, reversibility and sensitivity of the sol-based optical sensor to ammonia gas in a flow system, experiments were performed using the device shown schematically in Figure 3. The gas flow was switched between an ammonia/nitrogen mixture and pure nitrogen. When the ammonia gas was introduced for 35 min, the ammonia diffused into the xerogel film where deprotonation of the fluorescein dyes occurred, leading to a decrease in emission at 442 nm. The dyes in the xerogel were excited at 385 nm from the top of the gas sensor (Figure 2). The PMMA substrate acted as a waveguide and the fluorescence intensity was thus monitored at the edge perpendicular to the irradiation. The band pass filter only allowed light of wavelengths between 415 – 455 nm to pass to the photo detector. Thus, the change in fluorescence from 500 – 600 nm upon fluorescein deprotonation-protonation was not monitored. The emission was restored by flushing the system with pure nitrogen for 35 min to remove ammonia.

Figure 11a displays the response behaviour of 13.2 ± 2.9 µm 9.4 ± 1 µm and 6.3 ± 1.1 µm thick xerogel films towards 100 ppm ammonia. An undoped xerogel was measured as a reference and showed no decrease or increase in voltage when exposed to gaseous ammonia. The signal intensity increased from the thinnest to the thickest xerogel, consistent with the increasing absolute amount of dye immobilized in the films. For all film thicknesses, the first signal always was the most significant. The following cycles have symmetrical reversibility by exhibiting the same loss and recovery in signal intensity in each cycle except for the thickest 13 µm film, where a low continuous decrease in signal intensity was detected. This observation suggests that a certain amount of ammonia remained adsorbed by the xerogel even though the system was flushed with nitrogen for 35 min; this confirms the diffusion of the ammonia into the film. The recovery time is generally longer than the response time. This can be demonstrated using a higher ammonia gas concentration. Figure 11b shows that the rate of recovery time slows down with time. Scanning electron microscope and nitrogen-sorption experiments on the films revealed that the xerogels were not porous, which is certainly not beneficial to fast gas diffusion. A measurement to determine the response time was performed for each xerogel thickness with 100 ppm of ammonia. The response time (defined as the time required to achieve 95% of the maximum fluorescence signal decrease upon exposure to ammonia[10]) was 18 ± 2 min for the ≈6 µm xerogel film, 72 ± 7 min for the ≈9 µm xerogel film and 143 ± 12 min for the ≈13 µm xerogel film. This shows that the response time relates linearly to the film thickness. Preliminary studies showed that by using 13 µm xerogel layers 10 ppm ammonia can be detected with this experimental gas setup.

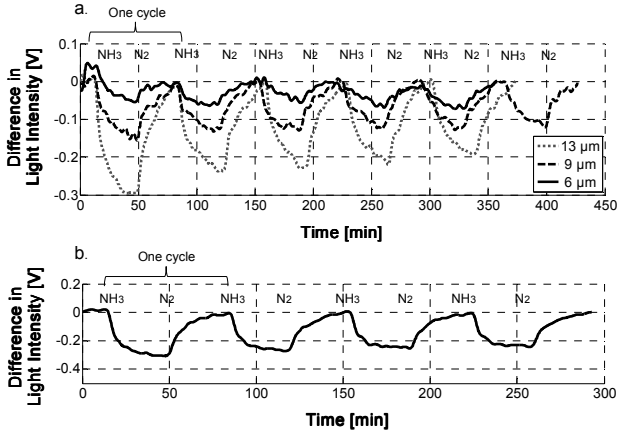

Fig. 11 a.: response and reversibility of the most sensitive (sol composed of 25 µmol coumarin and 6.25 µmol fluorescein) xerogel towards 100 ppm ammonia gas depending on xerogel thickness; b.: response and reversibility of a 6 µm xerogel to 1000 ppm ammonia gas.

4 Conclusion

This study demonstrates by means of an ammonia sensor system that the combination of two dyes can help to overcome problems regarding the non-linear response or sensitivity, which occur in sensor systems with only one fluorescent dye. In the presented system, the fluorescein acted as the ammonia trap, while the coumarin's emission signal was used to monitor the change of the ammonia concentration. This was only possible since coumarin and fluorescein form an energy transfer system. The much more pronounced decrease of the signal intensity made the FRET system highly advantageous for the quantitative analysis of a wide range of ammonia gas concentration.

The reversibility and practicability of the system was demonstrated with gas sensing experiments. Additionally, the cladding exhibited excellent long-term stability. Further studies to evaluate cross sensitivity with water and to improve the response time are planned to make a fully operating ammonia gas sensor possible. Since the pK_a values of the analyte sensing dyes determine the dynamic range of the sensor, dyes with lower pK_a values will also be investigated.

Acknowledgement

We gratefully thank M. Schmid and J. Gschwend and his workshop team for the implementation of our sensor designs. Additionally, we would like to thank M. Reber for the porosity measurements at the Zurich University of Applied Sciences.

Notes and references

[a] Empa, Swiss Federal Laboratories for Material Science and Technology, Laboratory for Protection and Physiology, Lerchenfeldstr. 5, 9014 St. Gallen, Switzerland. Fax: +41 58 765 74 99; Tel: +41 58 765 74 74; E-mail: Susanne.Widmer@empa.ch
[b] Department of Chemistry, University of Basel, Spitalstrasse 51, 4056 Basel, Switzerland
[c] IOS, Institute for environmental protection and sensors, Beloruska St. 7, Maribor, Slovenia.

1 B. Timmer, W. Olthuis and A. v. d. Berg, *Sens. Actuators, B*, 2005, **107**, 666-677.
2 P. C. A. Jerónimo, A. N. Araújo and M. Conceição B.S.M. Montenegro, *Talanta*, 2007, **72**, 13-27.
3 C. McDonagh, C. S. Burke and B. D. MacCraith, *Chem. Rev.*, 2008, **108**, 400-422.
4 X.-D. Wang and O. S. Wolfbeis, *Anal. Chem.*, 2012, **85**, 487-508.
5 S. Tao, L. Xu and J. C. Fanguy, *Sens. Actuators, B*, 2006, **115**, 158-163.
6 L. Peng, X. Yang, L. Yuan, L. Wang, E. Zhao, F. Tian and Y. Liu, *Opt. Commun.*, 2011, **284**, 4810-4814.
7 F. Galindo, J. C. Lima, S. V. Luis, M. J. Melo, A. J. Parola and F. Pina, *J. Mater. Chem.*, 2005, **15**, 2840-2847.
8 S. T. Yu Huang, *J. Sens. Technol.*, 2011, 29-35.
9 A. Persad, K.-F. Chow, W. Wang, E. Wang, A. Okafor, N. Jespersen, J. Mann and A. Bocarsly, *Sens. Actuators, B*, 2008, **129**, 359-363.
10 Y. Takagai, Y. Nojiri, T. Takase, W. L. Hinze, M. Butsugan and S. Igarashi, *Analyst*, 2010, **135**, 1417-1425.
11 F. Tavoli and N. Alizadeh, *Sens. Actuators*, *B*, 2013, **176**, 761-767.
12 K. Waich, T. Mayr and I. Klimant, *Talanta*, 2008, **77**, 66-72.
13 M. M. Martin and L. Lindqvist, *J. Lumin.*, 1975, **10**, 381-390.
14 R. Sjöback, J. Nygren and M. Kubista, *Spectrochim. Acta, Part A,* 1995, **51**, L7-L21.
15 H. Zheng, X.-Q. Zhan, Q.-N. Bian and X.-J. Zhang, *Chem. Commun.*, 2013, **49**, 429-447.
16 D. M. Goodall and D. R. Roberts, *J. Chem. Educ.*, 1985, **62**, 711.
17 T. Abel, B. Ungerbock, I. Klimant and T. Mayr, *Chem. Cent. J.*, 2012, **6**, 124.
18 C. Preininger, M. Ludwig and G. J. Mohr, *J. Fluoresc.*, 1998, **8**, 199-205.
19 Q. Chang, J. Sipior, J. R. Lokowicz and G. Rao, *Anal. Biochem*., 1995, **232**, 92-97.
20 K. Waich, S. Borisov, T. Mayr and I. Klimant, *Sens. Actuators*, *B*, 2009, **139**, 132-138.
21 J. Lei, L. Wang and J. Zhang, *Chem. Commun.*, 2010, **46**, 8445-8447.
22 E. P. Perman, *J. of Chem. Soc.*, 1901, **79**, 718-725.
23 E. P. Perman, *J. of Chem. Soc.*, 1903, **83**, 1168-1184.
24 H. Schmidt, *J. of Non-Cryst. Solids*, 1988, **100**, 51-64.
25 O. Lev, M. Tsionsky, L. Rabinovich, V. Glezer, S. Sampath, I. Pankratov and J. Gun, *Anal. Chem.*, 1995, **67**, 22A-30A.
26 C. Malins, T. M. Butler and B. D. MacCraith, *Thin Solid Films*, 2000, **368**, 105-110.
27 V. G. Parale, D. B. Mahadik, M. S. Kavale, S. A. Mahadik, A. Venkateswara Rao and S. Mullens, *J. Porous Mater*., 2013, **20**, 733-739.
28 B. J. Privett, J. Youn, S. A. Hong, J. Lee, J. Han, J. H. Shin and M. H. Schoenfisch, *J. Am. Chem. Soc*., 2011, **27**, 9597-9601.
29 R. M. Bukowski, R. Ciriminna, M. Pagliaro and F. V. Bright, *Anal. Chem*., 2005, **77**, 2670-2672.
30 C.-S. Chu and Y.-L. Lo, *Sens. Actuators*, *B*, 2008, **129**, 120-125.
31 C.-S. Chu and Y.-L. Lo, *Sens. Actuators*, *B*, 2007, **124**, 376-382.
32 R. Pardo, M. Zayat and D. Levy, *J. Photochem. Photobiol., A*, 2008, **198**, 232-236.
33 A. Lobnik, I. Oehme, I. Murkovic and O. S. Wolfbeis, *Anal. Chim. Acta*, 1998, **367**, 159-165.
34 A. Lobnik and O. S. Wolfbeis, *Sens. Actuators*, *B*, 1998, **51**, 203-207.
35 X. Chen, L. Lin, P. Li, Y. Dai and X. Wang, *Anal. Chim. Acta*, 2004, **506**, 9-15.
36 L. C. Klein, in *Sol-Gel Optics: Processing and Applications*, Kluwer, Boston, 1994, p. 7.
37 H. Kozuka, in *Handbook of Sol-Gel Science and Technology: Processing, Characterization and Applications*, vol. 1, *Sol-Gel Processing*, ed. S. Sakka, Kluwer, Boston, 2005, p. 338.
38 G. Palmisano, E. Le Bourhis, R. Ciriminna, D. Tranchida and M. Pagliaro, *Langmuir*, 2006, **22**, 11158-11162.
39 M. Pagliaro, G. Palmisano, E. Le Bourhis, R. Ciriminna, L. M. Ilharco and A. Fidalgo, *J. Nanomater.*, 2008, **2008**, Article ID 964046
40 J. D. Mackenzie, Q. Huang and T. Iwamoto, *J. Sol-Gel Sci. Technol.*, 1996, **7**, 151-161.
41 R. M. Almeida, in *Handbook of Sol-Gel Science and Technology: Processing, Characterization and Applications*, vol. 2, *Characterization and properties of sol-gel materials and products*, ed. S. Sakka, Kluwer, Boston, 2005, p. 68-77.
42 H. Leonhardt, L. Gordon and R. Livingston, *J. Phys. Chem.*, 1971, **75**, 245-249.